J Appl Electrochem (2008) 38:817–825
DOI 10.1007/s10800-008-9516-4

ORIGINAL PAPER

Controlled stripping of aluminide coatings on nickel superalloys through electrolytic techniques

B. Bouchaud · J. Creus · C. Rébéré · J. Balmain · F. Pedraza

Received: 9 October 2007 / Revised: 7 February 2008 / Accepted: 7 February 2008 / Published online: 22 February 2008

Abstract Aluminide diffusion coatings are widely employed to improve the oxidation and/or the corrosion resistance of highly added value turbine components operating in harsh environments at high temperatures. Refurbishment of such components requires appropriate removal of worn coatings and of the corrosion products layer—usually an oxide scale. Stripping is mostly carried out using hazardous chemical baths of limited reliability. In this work, an alternative stripping method based on electrochemical techniques has been carried out at laboratory scale for CVD Al diffusion coatings on a directionally solidified Ni base superalloy. Both the galvanostatic and the potentiostatic modes have been investigated. Prior to them, in situ gas bubbling induced by cathodic polarization seems to be an effective way to remove the superficial oxide scales. Measuring the open circuit potential during the experiments allows easy monitoring of the progress of the selective dissolution of the different layers. Complete removal of the aluminide coatings is indicated by potential values similar to those of the substrate. The correlation between the electrochemical features and the surface state after stripping has been carried out by scanning electron microscopy (SEM), energy dispersive spectrometry (EDS) and X-ray diffraction (XRD). The electrochemical approach is a promising means to strip out surfaces in a selective and reliable manner.

B. Bouchaud · J. Creus · C. Rébéré · J. Balmain · F. Pedraza (✉)
Laboratoire d'Etudes des Matériaux en Milieux Agressifs (LEMMA, EA 3167), Université de La Rochelle, Avenue Michel Crépeau, La Rochelle cedex 01 17042, France
e-mail: fpedraza@univ-lr.fr

Keywords Aluminium diffusion coatings · Electrochemical stripping · Galvanostatic and potentiostatic modes · Cathodic polarization

1 Introduction

In order to increase the lifetime and/or the operating temperature of turbine components, aluminide coatings are becoming a key factor to improve the corrosion/oxidation resistance at high temperatures of Ni-base superalloys through the formation of a continuous, adherent and slowly growing alumina scale [1–5]. However, the strongly aggressive environments [6–9] lead to Al depletion by spalling of the alumina scale due to thermal cycling and by interdiffusion into the substrate [10–12]. This can result in breakaway and enhanced corrosion and oxidation, hence in loss of the protectiveness provided by such coatings [4, 13, 14]. For high added value components, the removal of the defective oxide layers and worn coatings is required prior to the refurbishment and recoating operations. The stripping processes thus require effective and reliable removal of the superficial layers while maintaining the integrity of the underlying superalloy substrate as it must ensure the mechanical performance of the component.

Mechanical processes [15, 16] such as machining, grinding, polishing or blasting have been shown to be efficient to remove surface products but the components surfaces are subjected to local and intense deformation [17]. Therefore, coatings removal is typically performed using chemical baths, mainly composed of a combination of strong oxidizing reagents (e.g. $(NH_4)_6Mo_7O_{24}$, $7H_2O$, $K_2Cr_2O_7$) and very strong acids (e.g. HF, HNO_3) that may degrade the superalloy substrate [e.g. 18, 19]. Furthermore, most of these chemicals are toxic and carcinogenic [20].

Another method [21] consists in a mixture of inorganic acid (e.g. HCl) and an organic solvent (e.g. C_2H_5OH) to temper the stripping reactivity towards the substrate. This method leads to a good state of the stripped surface but some pitting corrosion of the uppermost surface may occur because of the chloride ions. Some other recent environmentally friendly and soft chemical stripping approaches have been discussed in the literature [22] but like any other chemical method they are not selective enough. However, the electrochemical stripping approach has been shown to be rather selective [23] to remove PVD CrN deposited from tool steel using alkaline electrolytes. The group of de Damborenea [24] also investigated the electrolytic removal of monolayers and mutilayers based on CrN and underlined the ease of monitoring the dissolution process. Using X-ray photoelectron spectroscopy (XPS), the authors also described the mechanisms of galvanostatic stripping [25]. In the case of aluminised Ni superalloys, only one work has been reported to strip part or a full component by imposing a current (i.e. using the galvanostatic method) in an electrolyte composed of inorganic acids and NaCl to increase the conductivity of the electrolyte [26]. However, the analytical methodology has not been fully explained nor the potentiostatic route discussed.

In this work, an alternative electrochemical stripping method based on a strong oxidizing inorganic acid, a pitting agent and a number of complex inorganic molecules providing high electrical conductivity is presented to selectively remove the oxide scales and the CVD-aluminide coatings on a directionally solidified Ni-base superalloy using galvanostatic and potentiostatic approaches. Analytical monitoring is carried out after each dissolution step, i.e. upon the stripping process itself. The methodology to remove efficiently such surface products is discussed in terms of the electrochemical dissolution charge and the results are confirmed using SEM/EDS and XRD.

2 Experimental

2.1 Samples

The substrates were 12.5 mm diameter and 1.3 mm thick discs of a directionally solidified (DS) Ni-base superalloy, whose nominal chemical composition is given in Table 1. The specimens were aluminised using current SIFCO Turbine Components CVD procedures at 1,050 °C for 6 h to produce the NiAl intermetallic compound on the additive layer.

Table 1 Nominal chemical composition of the directionally solidified substrate (at. %)

Ni	Cr	Co	Mo	W	Ta	Re	Hf	Al
60	8	12	1	1.5	2	1	0.5	14

2.2 Oxidation of the aluminide coated material

The aluminised specimens were cyclically oxidised in a muffle furnace for a period of 24 h intervals up to 240 h at 1,100 °C. Cooling took place rapidly from the oxidising temperature to room temperature. In contrast to standard testing [27] using short dwell times, this cycle was chosen to promote the interdiffusion of the coating elements to deplete the Al reservoir. It also aimed at inducing cracking of the alumina oxide scale because of growth and thermal cyclic stresses [12, 14].

2.3 Microstructural characterisation

The plan view and cross section coating microstructures were investigated by electron microscopy in the secondary electron and backscattered electron modes in a high vacuum JEOL 5410LV SEM with a coupled Rontec detector to perform EDS elemental microanalysis. Accurate analyses of the oxidised samples were performed in a Field Emission Gun FEI Quanta 200 F apparatus at 0.90 mbar to reduce the blurring effect of the non conductive alumina scales developed on the surface. A nickel electroless (Buehler) deposit was realised to protect the oxide scale from spalling during the metallographic preparation for cross-sectional studies. The efficiency of stripping was also monitored by XRD in a BRUKER AXS D8 Advance apparatus using CuK_α radiation in the θ–2θ configuration. Probing of superficial oxide scale was also performed by XRD at 3° glancing incidence (GIXRD). Assessment of the diffracting species was performed using DIFRAC^{plus} software.

2.4 Electrochemical features

The electrochemical stripping tests were carried out using a conventional three-electrode cell. It consisted in a Saturated Calomel reference Electrode (SCE) surmounted by a Luggin extension, a platinum Counter Electrode (CE) and the samples as the Working Electrode (WE). The average immersed area of the samples was about 3 cm^2. The experiments were performed using a Princeton Applied Research Potentiostat/Galvanostat 263A monitored by the SoftCorr III software.

The chemical composition of the stripping bath is confidential but must contain at least a strong oxidizing

inorganic acid (preferably from group XV of the Periodic Table), a pitting inorganic agent (preferably containing anions from the group XVII) to pierce the passive film that the aluminide coating forms in contact with the electrolyte and a number of complex inorganic molecules (preferably containing cations of the transition metals group) providing high electrical conductivity upon their dissociation in the water-based solution. Also, the dissociation of the complex inorganic molecules can result in the formation of strong reducing cationic species that can be complexed with the anions of group XVII allowing buffering of the dissolution rate of the metallic surface. For this to happen, the pH of the bath must remain strongly acidic (pH $<<$ 1). The stripping tests were realised at room temperature. The electrochemical behaviour of the samples in the baths was analyzed by cyclic polarization curves sweeping from a potential of -1 V/SCE to 2 V/SCE at a 20 mV s^{-1} rate and then the reverse polarization to -1.5 V/SCE. The open circuit potential (o.c.p.) measurements allowed the material behaviour and its capacity to form a stable passive film to be monitored. The electrochemical features were determined using the Tafel method. Both potentiostatic and galvanostatic tests were performed based on the existing potential differences between each phase present in the scale/coating/substrate system.

Before and after immersion in the stripping baths, the samples were cleaned in an ultrasonic bath of ethanol and subsequently dried with tangential hot air. Thereafter, they were weighed in a 10^{-5} g accurate Precisa XR205SR-DR balance in order to estimate the mass loss, hence the removed coating thickness.

3 Results and discussion

3.1 Coatings features

Figure 1 shows the structure and composition profile of the as-deposited aluminide coatings. The coating has the typical bi-layered morphology of an outwardly grown coating [e.g. 28] with the homogeneous additive layer on top and the interdiffusion layer underneath. The EDS profiles suggest the major formation of NiAl and of Ni_3Al at the additive and the interdiffusion layers, respectively. Moreover, local increases of the refractory element contents in the interdiffusion layer are normally ascribed to carbides and/or to topologically closed-packed phases (TCP) precipitation [29–31], which may subsequently exert an influence on the electrochemical stripping.

After cyclic oxidation at 1,100°C for 3 cycles (72 h in hot air), a heterogeneous oxide scale appears with spalled areas, cracking and nodule formation from oxygen inward diffusion (Fig. 2a). The chemical composition (Fig. 2b) also evolves significantly with the Al and Ni profiles flattening across the whole additive layer and half the interdiffusion layer. An increase of refractory elements at the interdiffusion layer occurs [30–33]. The β-NiAl to γ'-Ni_3Al transformation indicated by the bright contrasted areas occurs underneath the oxide scale and at the interdiffusion layer and implies Al depletion in such areas. Such cross section heterogeneities and the surface cracking and spallation may allow the electrolyte to permeate through upon stripping. The differences in chemical composition allow modification of the electrochemical potential of each phase and hence selective stripping.

The XRD patterns depicted in Fig. 3 confirm the previous observations. They indicate the single peak associated with the uncoated directionally solidified substrate, the three main peaks associated with the NiAl phase of the as-deposited coating and other peaks related to the α-Al_2O_3 oxide scale, NiAl and the Ni_3Al contribution from the NiAl $\rightarrow$ Ni_3Al transformation of the coating after 72 h (3 cycles) of oxidation. Such patterns can be employed as references to survey the surface state after each stripping batch.

3.2 Electrochemical characterisation

The effect of the electrolyte concentration plays a key factor on the stripping efficiency. Indeed, the coating should undergo uniform dissolution while leaving the

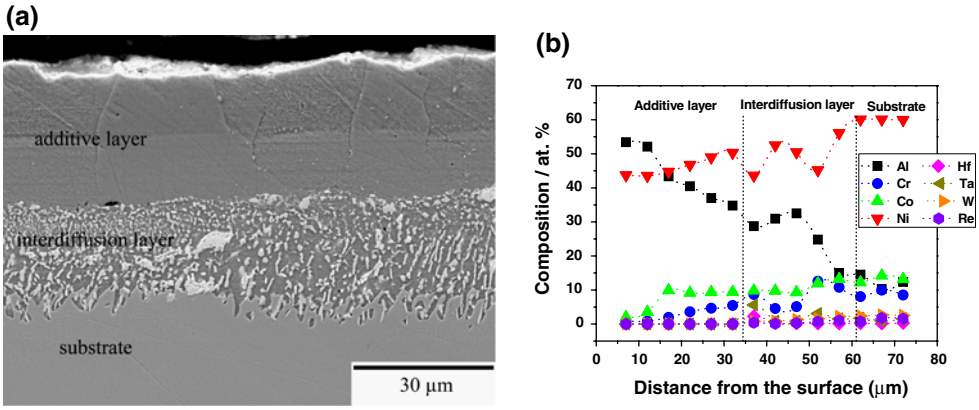

Fig. 1 (**a**) SEM cross-section of the coated substrate with Al by CVD at 1,050°C for 6 h and (**b**) EDS composition profile

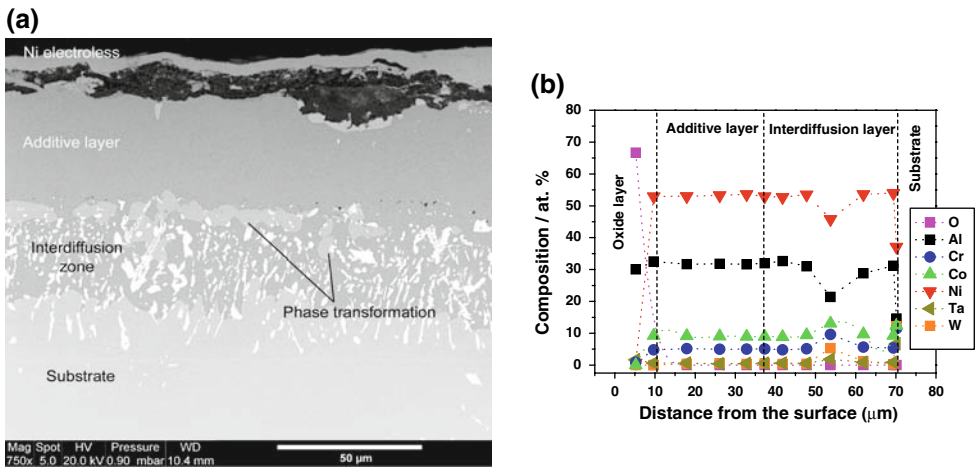

Fig. 2 (**a**) SEM cross section of the coated specimens after 3 cycles (72 h hot gas) of oxidation at 1,100°C in air and (**b**) the corresponding EDS composition profile

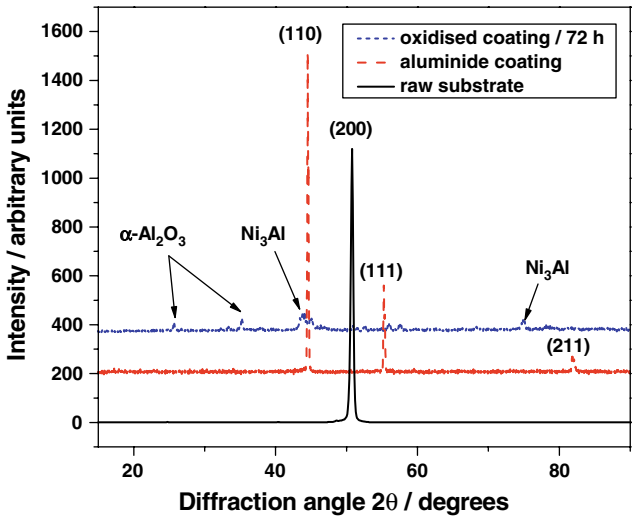

Fig. 3 XRD patterns of the raw substrate, CVD coating and coating after 72 h (3 cycles) of high temperature oxidation

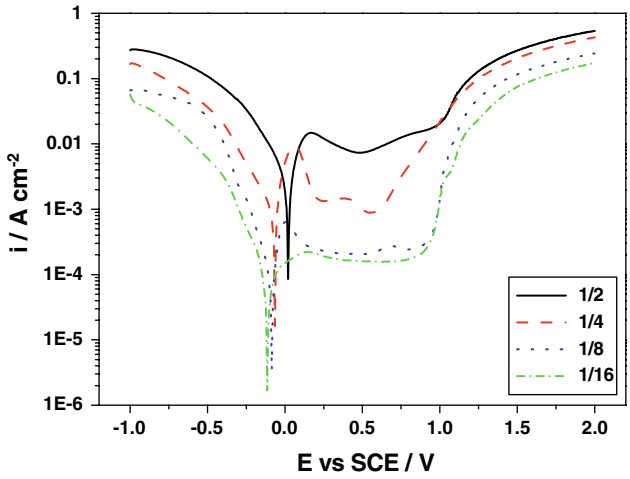

Fig. 4 Effect of the dilution of the electrolyte on the raw substrate using cyclic polarization curves (SR = 20 mV/s)

substrate unattacked. To this end, the ratio of the more active constituents was left constant and only the water content was progressively increased. The pH obviously increased with dilution but remained strongly acidic (pH $\leq$ 1) to ensure the stability of the reducing cation species. The conductivity dropped to about 95 mS cm^{-1} for the strongest (1/16) dilutions. Without any dilution, the samples were extensively attacked and pitted, undergoing significant mass losses. However, progressive dilution tended to moderate the attack (dissolution kinetics) of the substrate as shown in Fig. 4 (for the sake of clarity, only the ongoing sweep is plotted). The main electrochemical features deduced from these curves are gathered in Table 2. The reverse potential E_{rev} measured during the reverse scan gives information on the stability of the corrosion products developed on the sample surface, hence on the likely degradation of substrate.

In particular, the anodic branches show that the strong dissolution peaks fade with dilution as the surfaces become oxidised (passsivated). The undulations can be ascribed to combined cycles of corrosion and passivation of the surface. These cycles tend to disappear with the increase in water content, i.e. the passive domain broadens. This may allow stripping of the coating in a selective manner without altering the superalloy substrate. Moreover, some gas bubbling occurs in the cathodic domain probably from the hydrogen evolution reaction (HER). For the weakest dilutions (1/2 and 1/4), the current densities are the highest and therefore can still result in a significant degradation of the substrate and may not allow precise stripping control. Similarly, the transpassive domain is reached at about 600 mV vs. SCE leading to pitting corrosion. This overlaps with the water oxidation reaction at about 800 mV vs. SCE. The reverse scanning (not shown) follows a hysteresis for high anodic potentials and a strong shift of the reverse potential towards more cathodic potentials. In contrast, for the strongest dilution (1/16), there is no such transpassive domain and only the water oxidation reaction

Table 2 Summary of the major electrochemical features in the diluted stripping baths

	Bath	E_{corr} vs. SCE/mV	i_{corr}/mA cm^{-2}	E_{rev} vs. SCE/mV	i_{rev}/mA cm^{-2}
Raw substrate	1/8	−85	0.6	530	0.2
	1/16	−135	0.6	660	0.1
As-coated	1/8	−215	10	−235	6
	1/16	−215	2	−265	1
Oxidised coating	1/8	−180	3	−250	3
	1/16	−200	0.5	−260	2

becomes significant from 800 mV vs. SCE. With 1/8 dilution, limited transpassivation appears. The reverse scan confirms the stability of the passive film with a higher reverse potential. Because of the electrochemical passivity of the raw substrates in the electrolytes diluted by 1/8 and by 1/16, these baths were retained in the following to characterise the electrochemical behaviour of both the coated and oxidised coated substrates.

The characteristic shape of the polarization curves of the coated substrates for the strongest dilution factors is plotted in Fig. 5 (reverse scan not shown) and the electrochemical characteristics are given in Table 2. The corrosion potentials (E_{corr}) of the coated specimens are lower than the E_{corr} of the raw substrate. Also, for high anodic potentials ($E > 0$), higher current densities are registered especially at 1/8, which allow uniform dissolution of the coating while maintaining the integrity of the substrate. In both cases, during the reverse scan a slight hysteresis and a shift of the reversible potential towards more cathodic potentials may induce surface roughness.

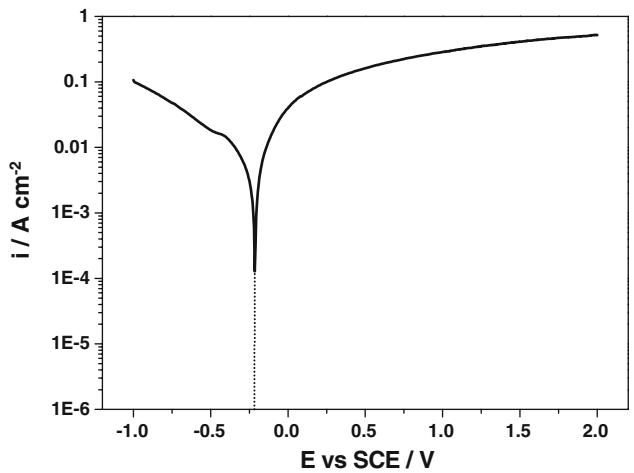

Fig. 5 Characteristic-shaped polarisation curve obtained on the aluminised substrate immersed in the stripping baths for the strongest dilution factors (SR = 20 mV s^{-1}). Similar trend for the coated and oxidised samples

Before testing the electrochemical behaviour of the oxidised coated substrates, a cathodic polarization procedure at −0.4 V vs. $E_{o.c.p.}$ for 15 min was carried out to remove the outermost oxide scale. After the cathodic polarization, the X-ray patterns exhibit no remaining peaks characteristic of α-Al_2O_3. Owing to the HER, hydrogen bubbling leads to the removal of the whole oxide scale over the surface of the samples hence eliminating the need for typical sand blasting operations before stripping. Once the upper oxide layer has been removed, the shapes of the curves are similar to those of unoxidised coated substrates with relatively different corrosion potentials as shown in Table 2 because of the NiAl to Ni_3Al transformation of the coating after oxidation (Fig. 3). This clearly shows the selectivity of the process as opposed to the chemical stripping methods.

The dilution by 1/8 brings about a larger passivity domain of the raw substrate and is nobler than in the 1/16 bath (ΔE_{corr} = +50 mV), and the coated and the oxidised coated substrates also show higher corrosion current densities than the raw superalloy. Therefore, only the 1/8 electrolyte will be studied in the following stripping experiments.

3.3 Electrolytic stripping

3.3.1 Galvanostatic process

The stripping process studied consisted in a combination of cathodic polarization, allowing removal of the oxide scale through the HER and the mechanical effects induced by bubbling of this gas, followed by anodic polarization inducing the dissolution (enhanced corrosion) of the coating. The open circuit potentials (o.c.p.) were measured before and after each stripping step to provide information on the surface state hence on the progress of the dissolution.

Using Faraday's law (Eq. 1), the surface dissolution charge to dissolve a thickness "*e*" of the coating can be calculated, assuming that the coating is mainly composed of Ni_3Al phase—matrix of the interdiffusion layer and bright contrasted areas of Fig. 2a—after oxidation.

$$\Delta m = \rho_{Ni_3Al} \times e \times S = \rho_F \times \frac{M_{Ni}}{nF} \times Q \quad (1)$$

where Δm is the mass loss, M_{Ni} the mass of nickel (58.69 g mol^{-1}), ρ_{Ni_3Al} the density of the aluminide coating (8.07 g cm^{-3}), e the thickness of coating, S = the sample electroactive area, n the number of electrons exchanged during the dissolution of the main element, F the Faraday constant (96500 C), Q the dissolution charge and ρ_F the Faradaic yield.

The surface dissolution charge can then be given by Eq. 2:

$$Q_S = \frac{Q}{S} = \frac{\rho_{Ni_3Al} \times e \times nF}{\rho_F \times M_{Ni}} \quad (2)$$

The total dissolution charge estimation is related to Faraday's law (Eq. 2) assuming that the yield is not higher than 75%. This dissolution charge can be fully applied in a single step. However, better process control is obtained by applying small charge steps followed by o.c.p. measurements to monitor stripping after each step. Concurrent evolution reactions may however reduce further the Faradaic yield and need also to be considered in the full assessment.

According to Fig. 6, the threshold current density is about 0.1 A cm^{-2}. Overpotentials could lead to water breakdown (Eq. 3), which may enhance dissolution of the coating (Eq. 4), thus bringing about a decrease in Faradaic yield. Indeed, the oxygen evolution reaction at the surface may form a barrier of oxygen bubbles that reduces the electroactive area in contact with the electrolyte thus leading to uneven dissolution of the coating. Therefore, according to Eq. 2, an increase in total dissolution charge is required.

$$2\ H_2O \rightarrow O_2 + 4H^+ + 4e^- \quad (3)$$

$$M \rightarrow M^{n+} + ne^- \quad (4)$$

The o.c.p. evolution during the galvanostatic stripping (Q_S = 180 C cm^{-2}) is given in Fig. 7. Before stripping (Fig. 7a), the $E_{o.c.p.}$ values stabilise at about −208 mV vs. SCE, in agreement with the previous results for the oxidised coatings. After stripping, the $E_{o.c.p.}$ values (about −190 mV vs. SCE) get closer to those of the raw substrate. Such o.c.p. increase can be ascribed to the active dissolution of the coating during the experiment.

After stripping, the XRD patterns confirm the disappearance of the alumina scale. Most of the peaks correspond to the Ni_3Al, carbides and TCP phases of the interdiffusion layer and a weak signal from the substrate. This indicates that the Faradaic yield is lowered because of electrical losses in the experimental set-up and of concurrent chemical reactions. Among the latter, the major loss arises from the initial complexation of the cationic species with the anions of group XVII that require a significant number of electrons to destabilize the complex, hence to release enough pitting anions and reducing cations. Therefore, the total dissolution charge needs to be increased, i.e. further cathodic/anodic steps are required. With a higher value of Q_S (Q_S = 204 C cm^{-2}) the $E_{o.c.p.}$ stabilises at −180 mV vs. SCE (Fig. 7b). This means that the fraction of dissolved coating is higher and therefore the o.c.p. tends to that of the raw substrate. Indeed, the relative intensity of the only XRD peak of the raw substrate with respect that of Ni_3Al and the carbides and TCP phases (unlabelled) is more important (Fig. 8).

The SEM top view and cross-sections micrographs correlate well with the observed differences. At low Q_S, only part of the additive layer has been fully removed whereas at increased Q_S values, the dissolution of the coating is almost complete (Fig. 9a and b). Therefore, an

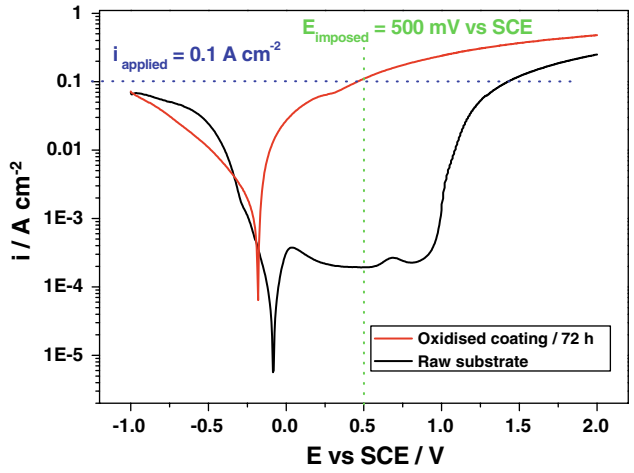

Fig. 6 Polarisation curves of both the raw substrate and oxidised coating immersed in the bath diluted by 1/8 (SR = 20 mV s^{-1}) and the applied current density and potential to perform stripping in the galvanostatic and the potentiostatic mode

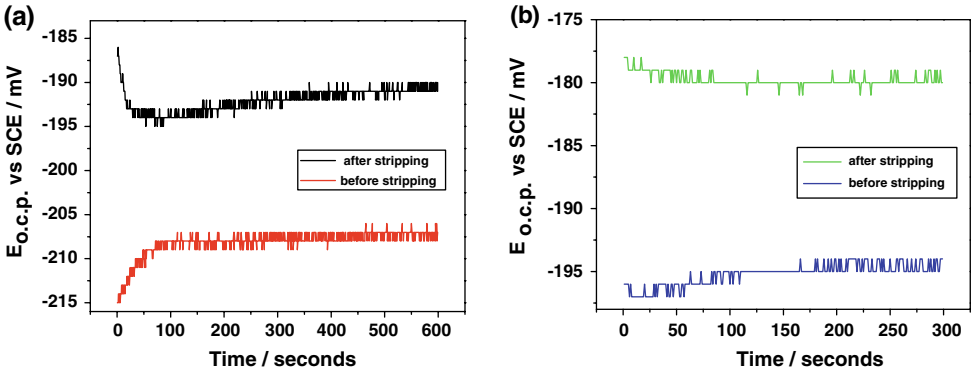

Fig. 7 (**a**) $E_{o.c.p.}$ evolution during galvanostatic stripping with (**a**) Q_S = 180 C cm^{-2} and (**b**) a higher Q_S (204 C cm^{-2})

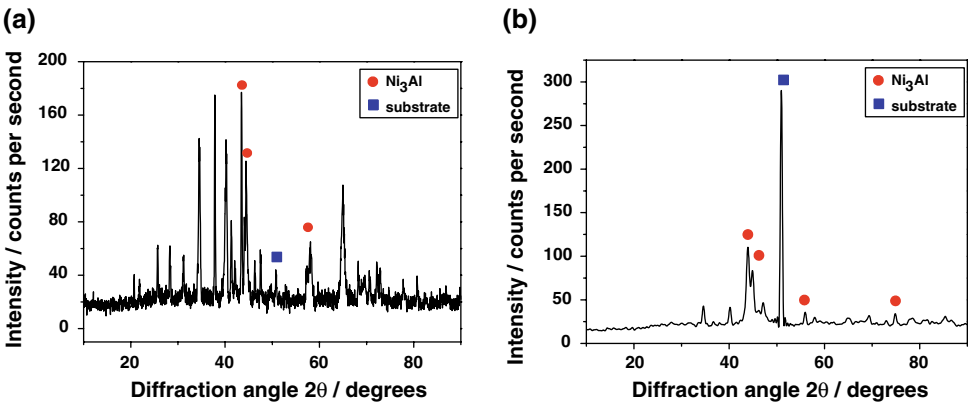

Fig. 8 XRD patterns of the stripped samples using the galvanostatic mode when applying different dissolution charges: (**a**) $Q_S = 180$ C cm^{-2} and (**b**) $Q_S = 204$ C cm^{-2}

assessment of the total dissolution charge is required while designing the stripping procedure and this can be easily adjusted by monitoring the open circuit potential of the samples.

Another goal of stripping is to produce relatively flat surfaces. However, the galvanostatic mode has been shown to produce relatively rough surfaces (Fig. 9c). This is mostly due to the dissolution mechanisms themselves. First, dissolution occurs selectively based on the potential differences between the layers and the phases across the coating. Once some phases are preferentially dissolved, a heterogeneous distribution of the current density lines appears at the electrolyte/samples electroactive area interface. Such lines concentrate mainly on narrow thin surface defects and/or heterogeneities thus leading to pronounced dissolution. This may compromise the application of the galvanostatic mode in complex geometries such as the actual turbine blades. Therefore, a second approach has been investigated using the potentiostatic mode likely to favour a better charge distribution over the samples surface, hence to promote stripping homogeneity and relatively flat surfaces.

3.3.2 *Potentiostatic process*

The potentiostatic mode consists in applying a potential, where the substrate is in its passive domain while the coating undergoes a uniform dissolution. According to Fig. 6, potential values of +500 mV vs. SCE seem to fulfil this requirement. As with the galvanostatic mode, the cathodic polarization followed by anodic dissolution steps were repeated until a potential value close to the one of the raw substrate was reached.

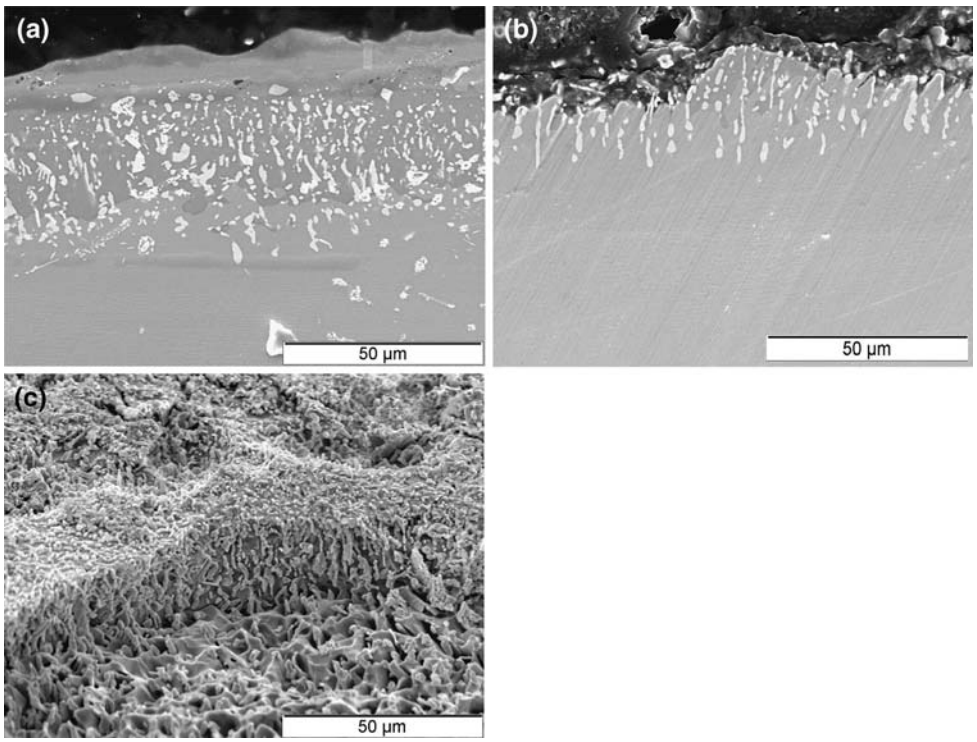

Fig. 9 (**a**) SEM cross section morphologies after the galvanostatic stripping when applying (**a**) $Q_S = 180$ C cm^{-2} and (**b**) $Q_S = 204$ C cm^{-2}. (**c**) SEM tilted (60°) view of the rough stripped surface using the galvanostatic mode (here for $Q_S = 204$ C cm^{-2})

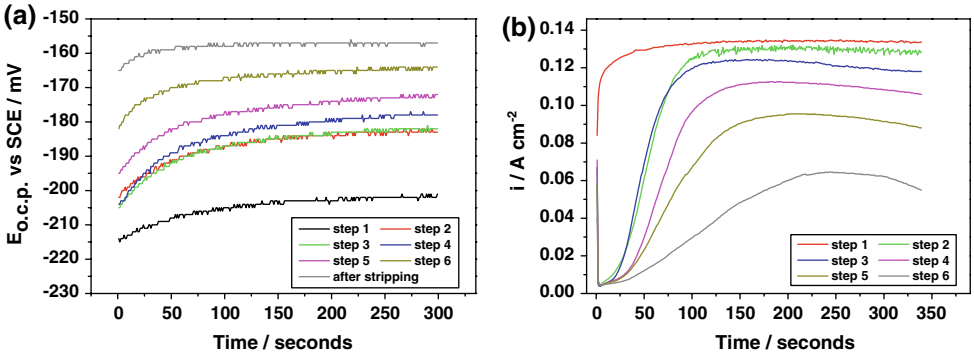

Fig. 10 Evolution of the (**a**) $E_{o.c.p.}$ and (**b**) the current density with the number of stripping steps using the potentiostatic mode

The $E_{o.c.p.}$ and the current density evolution during the stripping process are given in Fig. 10a and b, respectively. After the first step, the $E_{o.c.p.}$ values stabilise at about −205 mV vs. SCE, which is close to the originally oxidised coated substrate. Then, after the second step, a significant increase in potential occurs, which can be ascribed to the effective removal of the oxide scale. Subsequent cathodic polarization/anodic dissolution steps brings about an increase of the $E_{o.c.p.}$ in a more even manner. Simultaneously, during the first step, the current density increases rapidly, then stabilises at about j = 0.13 A cm^{-2}. With such current density, the coating enters in its active dissolution domain (see Fig. 6). Thereafter, by increasing the number of steps a decrease in current density progressively occurs. The solution enters into contact with the successive layers until the substrate is reached (step 6). At that point the current density is about 0.06 A cm^{-2} and the $E_{o.c.p.}$ value is about −160 mV vs. SCE, which is closer to that of the raw superalloy substrate.

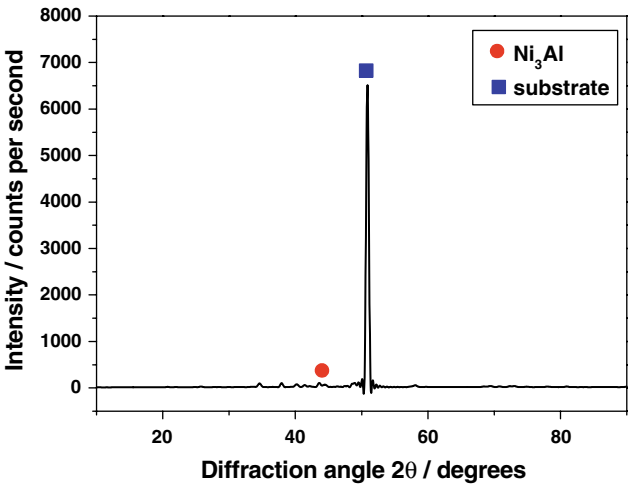

Fig. 11 XRD pattern of the stripped samples using the potentiostatic mode

Indeed, the diffractogram given in Fig. 11 shows that the main contribution comes from the substrate. Only a few small peaks from Ni_3Al, carbides and TCP phases (the 2 latter unlabelled) in the coating are still present. This is confirmed in the SEM surface and cross section inspections (Fig. 12), in which the typical γ/γ' microstructure of the superalloy substrate is present together with a number of TCP precipitates. The remaining thickness of the interdiffusion layer is less than 10 μm and is therefore acceptable for subsequent refurbishment operations [32]. It seems therefore that the potentiostatic mode allows stripping in a more homogeneous and selective way than the galvanostatic mode.

4 Summary and conclusions

Stripping tests of a directionally solidified Ni-base superalloy, uncoated, coated and coated and oxidised at high temperatures have been carried out using an electrochemical approach. The method is based on the differences in the

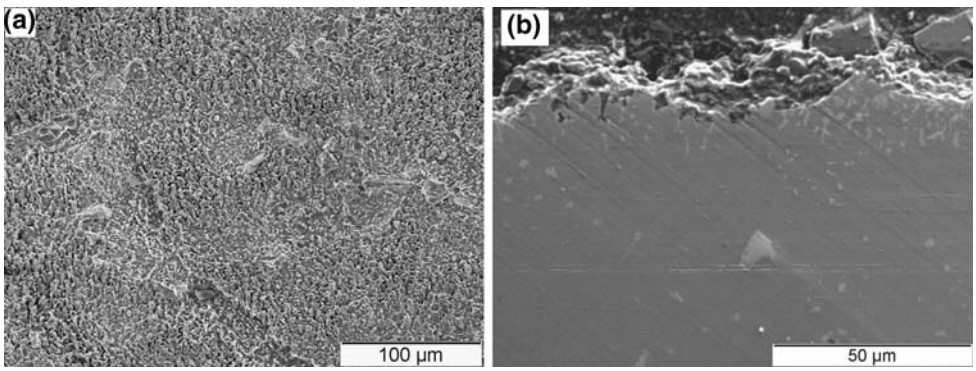

Fig. 12 (**a**) SEM surface and (**b**) cross section morphologies of the stripped samples using the potentiostatic mode

electrochemical potential among the various layers and phases. Electrochemical characterisation allows selection of the appropriate dissolution conditions from strongly acidic solutions of high electrical conductivity. The solutions tested contained a strong oxidizing acid, a pitting agent and a number of complex inorganic molecules which buffer the dissolution rate. Selective removal of the oxide scales and the eventual passive films can be undertaken in situ by imposing a cathodic potential that induces hydrogen reduction and bubbling. Thereafter, either galvanostatic or potentiostatic modes dissolve the underlying coating. Application of the galvanostatic mode requires careful assessment of the Faradaic yield because the complexation phenomena in the bath must be considered and a significant amount of electrons must be employed to destabilize the complex, hence to release the reducing cations and pitting anions required in the process. Also, electrical losses occur due to the uneven distribution of the current lines in. As a result, the stripped surfaces look rougher compared to samples stripped in the potentiostatic mode. In contrast, for the same time of processing (number of steps), the potentiostatic mode dissolves the coating in a more even manner. Regardless of the mode, the stripping can be monitored in situ by measuring the $E_{o.c.p.}$ after each removal step. The process is completed when the $E_{o.c.p.}$ is close to that of the raw superalloy substrate. The electrochemical results are supported by XRD and SEM observations. It can therefore be concluded that the electrochemical technique offers great dissolution selectivity and reliability.

Acknowledgments This work was partly sponsored by SIFCO Turbine Components. The authors are greatly indebted for their contribution, substrate and coating supply.

References

1. Beeley PR, Driver D (1984) Met Forum 7:146
2. Pedraza F, Tuohy C, Whelan L, Kennedy AD (2004) Mat Sci Forum 461–464:305
3. Haynes JA, Zhang Y, Cooley KM, Walker L, Reeves KS, Pint BA (2004) Surf Coat Technol 188–189:153
4. Evans HE, Taylor MP (1997) Surf Coat Technol 94–95:27
5. Van de Voorde MH (1984) In: Kossowsky R, Singhal SC (eds) Surface Engineering, Series E Applied Sciences No. 85. Martinus Nijhoff and NATO Scientific Affairs Division, Pittsburg
6. Eliaz N, Shemesh G, Latanision RM (2002) Eng Fail Anal 9:31
7. Giggins CS, Pettit FS (1980) Oxid Met 14:363
8. Goebel JA, Pettit FS, Goward GW (1973) Metall Trans 4:261
9. Mercier S, Iozzelli F, Bacos MP, Josso P (2004) Mat Sci Forum 461–464:949
10. Jedlinski J (2005) Mat High Temp 22:485
11. Pint BA, Tortorelli PF, Wright IG (2002) Oxid Met 58:73
12. Tolpygo VK, Clarke DR (1999) Surf Coat Technol 120–121:1
13. Littner A, Schütze M (2003) J Corr Sci Eng 6:78
14. Pérez FJ, Pedraza F, Hierro MP, Balmain J, Bonnet G (2002) Surf Coat Technol 153:49
15. Shipway PH, Bromley JPD, Weston DP (2007) Wear 263:309
16. Mosser MF, Kircher T, McMordie BG (1998) Patent EP-0861919
17. Kompella S, Moylan SP, Chandrasekar S (2001) Surf Coat Technol 146–147:384
18. Bowden JH, Conner JA, Rosenzweig MA (2000) Patent EP-1013797
19. Amirkhanova NA, Nev'yantseva RR, Bybin AA, Semenova IP, Smol'nikova OG (2003) Prot Met 30:487–489
20. EU Directive 2006/11/CE
21. Donald LSM, Sangeeta D, Rosenzweig MA (2000) Patent EP-1050604
22. Poupard S, Martinez JF, Pedraza F (2008) Surf Coat Technol (in press)
23. Sen Y, Ürgen M, Kazmanli K, Cakir AF (1999) Surf Coat Technol 113:31
24. Cristobal AB, Conde A, Housden J, Tate TJ, Rodriguez R, Montala F, de Damborenea J (2005) Thin Solid Films 484:238
25. Conde A, Cristobal AB, Fuentes G, Tate T, de Damborenea J (2006) Surf Coat Technol 201:3588
26. Fay W, Goodwater F, Updegrove K (2000) Patent US-6165345
27. COTEST Development of a code of practice for the characterisation of high temperature materials performance—5th EU Framework programme G6RD-CT-2001-00639
28. Angenete J, Stiller K (2002), Surf Coat Technol 150:107
29. Chen JH, Little JA (1997) Surf Coat Technol 92:69
30. Rae CMF, Hook MS, Reed RC (2005) Mat Sci Eng A396:231
31. Rae CMF, Reed RC (2001) Acta Mater 49:4113
32. Acharya MV, Fuchs GE (2004) Mat Sci Eng A381:143
33. Pedraza F, Kennedy AD, Kopecek J, Moretto P (2006) Surf Coat Technol 200:4032